Physica Scripta

PAPER

Optical parametric amplifier pulse cleaning driven by aperiodic frequency converter

To cite this article: Zaharit Refaeli *et al* 2022 *Phys. Scr.* **97** 075503

IOP Publishing Phys. Scr. 97 (2022) 075503 https://doi.org/10.1088/1402-4896/ac73bd

Physica Scripta

CrossMark

RECEIVED
16 March 2022

REVISED
16 May 2022

ACCEPTED FOR PUBLICATION
26 May 2022

PUBLISHED
7 June 2022

PAPER

Optical parametric amplifier pulse cleaning driven by aperiodic frequency converter

Zaharit Refaeli[1,2], **Gilad Marcus**[1], **Haim Suchowski**[3] **and Yariv Shamir**[2]

[1] Applied Physics Department, The Hebrew University, The Edmond J. Safra Campus - Givat Ram, Jerusalem, 9112001, Israel
[2] Applied Physics Division, Soreq NRC, 8180000, Yavne, Israel
[3] School of Physics and Astronomy, Tel-Aviv University, Ramat-Aviv 6997801, Tel-Aviv, Israel

E-mail: zaharitre@soreq.gov.il

Keywords: parametric amplifiers, pulse contrast, second harmonic, non-linear optics, ultrafast laser, aperiodicly poled crystal

Abstract

We demonstrate temporal shape improvement of a short laser pulse using chirped aperiodic nonlinear frequency converter within an optical parametric amplifier. The aperiodic converter generated walk-off free high spatial quality pulse with ~40% efficiency second harmonic while preserving the pump bandwidth. A <300 fs idler pulse was generated, with ~10 nm central wavelength tunability around 1053 nm by pump generation and phase matching control. A pronounced contrast pedestal suppression of up to 40 dB was observed within a few picoseconds range around the peak. Such pedestal suppression has good scalability potential to high energies.

1. Introduction

Interaction of extremely intense light with solids is of great importance for fundamental and applied research, such as generating high harmonics from solids [1], or heavy particle acceleration [2] from thin foils. Such experimental fields introduce the challenge of early-unwanted target response caused by imperfect pulse shape, allowing some energy to impinge on the target before the main peak. Therefore, high energy, femtosecond lasers based on chirped pulse amplification (CPA) [3] must exhibit excellent temporal contrast, namely, maintain a large ratio between the main pulse peak and some energy that is temporally dispersed away. These imperfections are generally caused by non-compensated dispersion, nonlinear phase, or noises. Contrast deteriorating mechanisms can be roughly divided into incoherent and coherent factors [4]. Amongst the first are noises, mainly amplified spontaneous emission (ASE) in amplifiers, or parametric fluorescence in nonlinear processes. Coherent factors are mostly higher-order dispersion, nonlinear phase accumulation, and scattering from optics imperfections. Although coherent factors are temporally deterministic, they manifest as erratic features in the near vicinity of a pulse peak, readily observed at the compression stage, and are difficult to eliminate. One element that had been reported to have such a coherent effect on contrast [4] is diffraction grating, practically found in any short pulse lasers either in the stretching or in the compressing stages. Since typical grating has huge sub-micron structures scribed on its surface (typically 1000 to 2000 lines/mm), slight imperfections introduce unwanted scattering and phase distortions, leading to time distortions in the compressed pulse. Moreover, as a result, this off-scattered energy is visualized while a contrast test is performed. Such tests are standardly displayed on a power-scale using pulse diagnostics tool, e.g. Frequency Resolved Optical Gating (FROG), or in a 3rd order autocorrelator. A typical trace that is attributed to the coherent scattering is a contrast pedestal (CP) [5, 6], featuring a skirt shape, ramping up and decaying pre and post to the main energy. Typically, the CP spans a few picoseconds (ps) to 10 ps around the main peak when displayed in the power scale versus time axis. This short-term CP was pointed out to be extremely hard to wipe out while maintaining a significant fraction of the pulse energy, whereas ASE noise is spread over a much longer-term and addressed separately. In this regard, directly addressing grating quality improvement showed ~1 order of magnitude CP suppression, obtained by adopting a transmission grating into the stretcher [6], claiming its manufacturing superiority. However, deploying transmission grating is not always applicable in some cases, like very high energies, requiring a different approach. In recent years, significant effort was invested in studying various techniques for handling pulse contrast deterioration. Controlling dispersion using grating stretchers and compressors is possible mainly up to the 2nd and 3rd orders, enabling their compatibility to improve pulse shape, thus improving pulse contrast [7, 8]. However, since these grating-based modules are controllable to that extent, their flexibility in handling fine structures within complex pulse shapes are limited. Recent advances in using highly negative dispersive chirped mirrors [8] showed the ability to enlarge compression capacity, which might open a path for further dispersion control. Another direction of handling coherent dispersion factors may emerge from a recent demonstration in microwave photonics, where interferometers inside optical fibers showed improvements in the output pulse quality, mainly in the 3rd order [9].

Overall, since the main energy lobe of ultrashort pulses occurs in the sub-picosecond timescale, suppression of delicate and very fast pulse features, formed by a combination of coherent and incoherent factors, is commonly handled via nonlinear gating processes, which are discussed in more detail in section 3. In this work, we mainly address the CP temporal regime via nonlinear parametric amplification and consequently time gating, based on the specialty fabricated crystal and short parametric amplifier, as elaborated below.

2. Motivation

At laser intensities of beyond 10^{10} W cm^{-2}, a solid target surface start to ablate into plasma, which easily reflects the incident beam, therefore, inhibiting desired interactions. However, more and more studies seek laser-matter interactions with intensities exceeding 10^{21} W cm^{-2}. With such intensities, even a small pre-pulse with only 10^{-7}–10^{-11} portion of the energy, could lead to surface ablation and prevent the interaction of the main pulse with the target. Therefore, improving the contrast ratio between pre-pulse and the main pulse, with emphasis on the CP regime, is of paramount significance.

Ultrafast intense lasers require multi-stage amplifiers that provide high energy and sufficient bandwidth simultaneously. Such a system can introduce unwanted temporal structures, originating from complicated dispersion and nonlinearities, both generated and amplified throughout the amplifiers chain. Moreover, some multi-stage laser amplifiers maintain more than a single stretching and compression stage, potentially inducing CP trace already at early stages. Thus, it can be of high interest to generate clean pulses with emphasis on lowering their CP, already in low energies, e.g. multi- nJ to μJ range for directly seeding further amplifiers.

Nowadays, the high-energy laser segment is dominated by Nd:Glass amplifiers, with energies of even multi kJ per amplifier [10]. Such lasers further emphasize the importance of contrast control with their huge energy gain factor (seed to final pulse gain of 10^{12}), where the amplified pulse accumulates pre/post pulses and other parasitic noises. This is the motivation for cleaning the pulse in the early amplification stages, potentially providing a simpler temporal phase structure in later stages and easing the compression process.

3. Contrast enhancement methods

Suppressing very short satellite pulses while leaving the main pulse unchanged necessitates some time-gating (or 'windowing') technique applied around the desired temporal part. Due to the extremely short temporal nature of femtosecond laser pulses, windowing based on, e.g. electronic based modules, generally confined to the ns time scales, cannot be used to enhance contrast. As a result, faster gating, only found in all-optic mechanisms, must be used. As elaborated below, such an approach can be applied mostly using nonlinear optical processes.

In recent decades, several techniques were developed to improve laser pulse contrast. Only a few to list include e.g. Saturable absorbers [11], Cross-polarized wave (XPW) [12], plasma mirrors (PM), optical parametric chirped pulse amplification (OPCPA), and specifically short optical parametric amplification (SOPA) [13], with intermediate compression for generating short pump and signal. All these techniques are based on instantaneous nonlinear gating mechanisms. In some cases, obtaining the desired contrast level (typically more than $>10^7$) necessitates a deployment of methods combination.

In SOPA, tight synchronization between pump and seed is achieved by taking both from a split point after the oscillator. Since the pump has to be more energetic than the seed, and as in most cases with a shorter wavelength, in many SOPA designs, the pump pulse is further amplified in a separate amplification chain and then frequency-doubled. In such a process, only the signal part that temporally overlaps with the pump is amplified.

Here we report on the improvement of pulse contrast in an early stage SOPA, planned for further feeding into a multi-stage high power OPCPA laser system. Naturally, intermediate compression implementation in SOPA can deliver some CP energy. Therefore, we explore the suppression of the latter, as a path to support reduced forward noise and CP amplification in higher energies.

When using SOPA with bulk nonlinear crystals and relatively low pump energies, several issues arise. First, in some nonlinear crystals, tight focusing is required to attain adequate gain, which reduces the effective interaction length between the three waves due to a short Rayleigh range, thereby limiting the overall efficiency. Second, such tight focusing increases the inherent problem of beam walk-off, sometimes reaching a few tens of milliradians, which with the combination of small beam waist generates an elliptical beam shape that is hard to handle. That may deteriorate the beam quality and disrupt further beam handling and proper amplification. In addition, a critical issue of using a short pulse duration pump is the inherent requirement to support a large phase-matching bandwidth, which is sometimes inconsistent with the demand for high and uniform gain. Specifically, large gain requires a relatively long crystal, which can introduce back conversion, parasitic optical parametric generation, and group velocity mismatch - all leading to partial bandwidth exploitation.

A different approach uses periodically poled crystals, designed to enable a tuning knob to the phase-matching curve via quasi-phase-matching (QPM), simultaneously solving the tight focusing and beam walk-off issues. However, the second harmonic generation (SHG) bandwidth using such a crystal is typically not very wide. Only in specific cases, e.g. broadband pump, or close to degeneracy with a certain dispersion design, larger gain bandwidth can be achieved in an OPG or OPA schemes [14, 15] rather than SHG.

To overcome the above-mentioned problems, we used here a modification of the latter in the form of Aperiodically Poled $LiNbO_3$ (APPLN) crystal to generate the required clean pump for a SOPA amplifier. At this stage, the material was selected for its availability and well-established processing among many manufacturers.

As opposed to birefringence and uniform period quasi-phase-matching, an aperiodic frequency converter (AFC) [16–19] gradually transfers the power between fields at different frequencies with a sweep of phase-mismatch between the interacting waves. The AFC process is an isomorph to adiabatic passage in a two-level atomic system transfers in this case, power between two fields over a broad bandwidth occurring near $\Delta k(z) = 0$. Additionally, there is no back-conversion, which is the case in standard crystals, thus it resolves the bandwidth-efficiency trade-off in nonlinear frequency conversion.

In AFC, the adiabatic parameter is the phase mismatch variation along with the optical axis $\Delta k(z)$. This parameter sweeps through $\Delta k = 0$, must be slow enough to result in an adiabatic transfer of energy between the interacting optical fields, namely to satisfy the adiabaticity condition [16]:

$$\left| \frac{d\delta k}{dz} \right| \ll \frac{(\kappa^2 + \Delta k^2)^{3/2}}{|\kappa|} \tag{1}$$

Where k is the wave-vector, z is the position along the propagation axis and κ is the nonlinear coupling coefficient between the three involving waves. Such a longitudinal variation of Δk can be designed in an aperiodically poled QPM grating. This simple adiabaticity appears when the phase-mismatched $\Delta k(z)$ varies linearly along with the crystal.

Recently, AFCs [20–22] showed conversion bandwidth far exceeding the ordinary phase matching, with spectrally flat efficiency, making it highly suitable for ultrafast systems. Furthermore, AFC can preserve high beam quality with a regular shape of incident beams, as walk-off is inherently canceled out, therefore, can be readily used in succeeding interactions. Both features make AFC highly attractive for this work.

In the past few years, there was also a tremendous advance in applying adiabatic OPA crystal to an OPCPA system, with further perfections demonstrated by U. Keller's group in 2010, with OPCPA amplification, albeit in the mid-IR [23, 24]. With this system, the first aperiodic QPM OPCPA was demonstrated [25, 26]. The fully nonlinear regime also received special attention in OPA and OPO [27–29].

4. Experimental approach

In this work, we integrate AFC inside a near-infrared (NIR) short OPCPA system. Where the deriving pump, an SHG beam, was generated via an AFC to demonstrate an idler with pronounced suppression of unwanted features and contrast improvement near the main pulse vicinity. The use of AFC provides an efficient, robust pump with minimal group velocity mismatch between the 1 μm pump and its second harmonic, and with the unique property of no back conversion, as previously reported [18, 19]. To synchronize the system perfectly, both pump and seed originated from the same oscillator. Firstly, the pump was split from the seed, amplified in two successive fiber amplifiers, and frequency-doubled by the AFC [16–19]. At the end of the beamline, the output beam from the AFC was mixed with a seed beam, facilitating the SOPA. The beam was analyzed via a second harmonic FROG device. The pre and post-contrast values were measured on the CPA and SOPA beams respectively in a 12 ps span window.

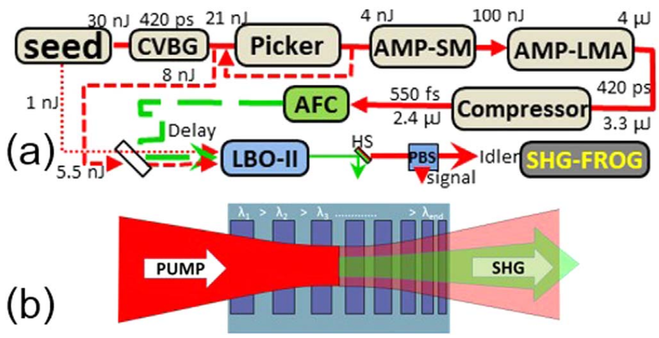

Figure 1. (a) System schematic. CVBG : Chirped Volume Bragg Grating, Small and large mode fiber amplifiers (AMP-SM and AMP-LMA respectively), HS: harmonic separator, PBS: polarization beam splitter, LBO-II: short OPA crystal. SHG-FROG: second-harmonic generation frequency-resolved optical gating pulse retrieval tool. (b) Schematic of the nonlinear aperiodic frequency converter (AFC) structure with aperiodic strips: pump IR (red) and SHG (green) beam crossing.

5. Experimental details

The system is an in-house build (figure 1(a)), starting from a 70 fs mode-locked oscillator operating at a central wavelength of 1.053 μm in 80 MHz pulse frequency (OneFive ORIGAMI-10-HP), providing $>$30 nano Joule (nJ) energy per pulse. The pulses from the seeder were split into two paths: one was stretched to ~420 ps and amplified to use as the pump, as elaborated below; The second facilitate the signal for the SOPA and was left slightly stretched (by preceding optics), which provided some better overlap with the pump beam in the nonlinear crystal. The stretching was obtained using Chirped Volume Bragg Grating (CVBG) with ~70% reflection efficiency and ~17 nm FWHM, super-Gaussian reflection spectrum. The reflected beam yielded a hard clipped ~12 nm linewidth pump in the fundamental harmonic. An acousto-optic pulse picker reduced the repetition rate to 1 MHz, leaving enough power to saturate the amplifiers. The pulses were directed into two successive Ytterbium (Yb) doped fiber amplifiers, a small and large mode area double-clad single mode types, separated by fiber isolator. Such amplifiers are superior in beam handling, thermal load, and quantum efficiency, however, intense pulse propagation in fiber can easily accumulate a nonlinear phase that can be manifested as poor pulse shape and contrast after compression. Therefore, even though $>$10 μJ energy could be extracted, we operated it up to 4 μJ. Both amplifiers were counter pumped by homemade, fully glass-integrated pump couplers with 976 nm diodes of ~2 W and ~10 W, respectively.

Prior to generating the pump, the fiber CPA beam was compressed via a grating compressor to ~600 fs as elaborated below. At the output of the CPA system, a Near-Gaussian beam with an M^2 factor of ~1.3 (figure 2(a)), and an estimated Gaussian fit of $>$98% in both axes were obtained.

Conversion to a second harmonic (526.5 nm) pump beam was done via a specialty designed AFC, serving as the pump beam for the OPA. It is stressed out that since the Yb-doped fibers possess the largest emission cross-section around 1030 nm, slight gain-shaping towards the shorter side was observed in the CPA beam in figure 2(b), yet left sufficient energy at the target wavelength. The pump and seed beams overlapped in a type-II Lithium Triborate (LBO) crystal for ease of polarization separation in a degenerated OPA to produce an extraordinarily polarized idler.

The separation of the pump from the signal and idler was done by a chromatic filter ($T_{SHG} = 0.25\%$, $T_{1\mu m} = 98\%$), followed by a polarizer (T_P:$T_S > 1000{:}1$) for signal–idler separation correspondingly. The resulted idler was obtained most efficiently at the point where a maximum signal/pump overlap was set using a delay line, as explained below.

The short-pulse OPCPA schematic is shown in figure 1(a). The pulses were transported to a grating pair Treacy type compressor [30] (1200 l mm^{-1} reflection gratings), then focused to ~200 μm and directed into the nonlinear AFC.

The pump was temporally synchronized with a micrometer stage delay line to generate the clean idler to overlap with a few (~5) nJ seed. The seed arrived from the unpicked port of the pulse picker and was recompressed inside the CVBG opposite side. This yielded a ~260 fs seeding signal. Considering the 11 nm hard-clipped spectrum modification produced by double passing the CVBG, (estimated FTL pulse duration of ~160 fs) the measured signal maintained some chirp naturally embedded in the transport optics. A slight additional chirp was purposely added to the signal using transmission-grating pair (1000 line/mm) to better overlap with the pump beam. This yielded ~500 fs pulses.

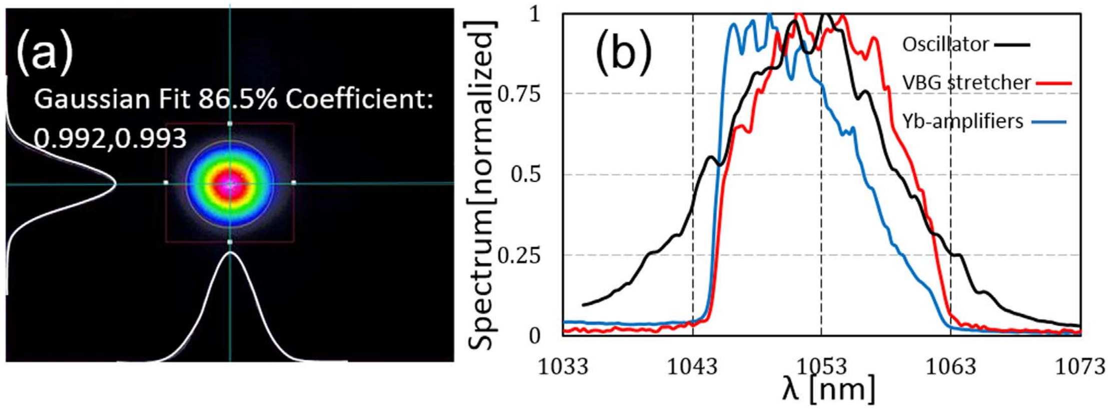

Figure 2. CPA output beam: (a) Beam profile out of the output coupler. (b) Measured spectrum of: seed laser (black), stretcher (red), and CPA output (blue), showing the stretcher's hard clip and Yb gain shaping.

6. Nonlinear converter design

The AFC crystal, based on $LiNbO_3$ was designed to match the spectrum of the amplified beam, centered around 1.05 μm, to produce the short SHG pump. We have used several AFC designs with 4 mm and 2 mm lengths, both with 1 mm height, wherein all, the poling structures were particularly designed to phase match bandwidth of 16 nm and to yield efficient and robust SHG pulses. It is worth noting that the very few-mm crystal length design was meant to tackle the two-photon absorption (TPA) of $LiNbO_3$, which for the SHG wavelength is constant of $\beta \sim 0.45$ cm kW^{-1} [31].

The output contrast of the OPA was pre-estimated by viewing the evolution equation of the pump, signal, and idler governed by the nonlinear coupled-wave equations in the time domain. Mostly under low gain conditions and undepleted pump approximation, the idler propagation equation yields intensities relation of the form [32]:

$$I_i \propto I_{s0} I_p \tag{2}$$

Where I_i, I_{s0}, and I_p stand for idler, initial signal, and pump intensities, respectively. In particular, if the pump pulse is the second harmonic of the signal, with contrast that is the square of its input signal, as realized in our system, the contrast of the generated idler is expected to be consistent with the cubic of the incident signal pulse.

7. Results

For the short OPA, the second nonlinear process was obtained using a type-II 25 mm long LBO crystal. A type-II scheme was selected for polarization separation of the degenerated signal/idler, and the small walk-off (~5.6 mrad). About ~730 nJ of the 526 nm SHG pump, was mixed with the 5 nJ re-compressed signal (higher energies were obtainable but involved unwanted thermal load). Following chromatic SHG separation, a polarizer cube separated the signal and idler. The energy of the output idler at 1053 nm was ~80 nJ, which is about 11% of the 730 nJ pump energy. Moreover, the idler wavelength could be shifted from 1043 to 1057 (figure 4(b)) with even better efficiencies by controlling the following parameters: delay, pump focusing and position, pump power, and LBO orientation. This property demonstrated good spectral flexibility embedded in the OPCPA system based on the use of AFC structure. In such way, up to 130 nJ were obtained at the vicinity of 1045 nm (~18% of the pump), mainly due to the slight red-shift gain shaping of the amplifiers. A broad idler with 10.9 nm FWHM (figure 4(a)) was achieved due to the broad pump conversion in the AFC (figure 3(a)).

In order to have some more clear view of the demonstrated technique, the following table was prepared. Typical beam parameters of AFC, designed in this case for SHG process (as obtained from figure 3), as compared with other well-established frequency conversion techniques, a Barium Borate (BBO) and Periodically poled Lithium Niobate (PPLN). The three techniques are presented in table 1 under similar spectral widths and energies.

As can be inferred from table 1, the combination of efficiency, bandwidth preservation and spatial beam quality is advantageous in using AFC over the other approaches and is explored here only preliminary.

The enabled spectral flexibility in this system consequence the pump linewidth and phase matching width of the short OPA stages. This flexibility can be utilized for further broadband amplifiers, compatible with several lasing materials, e.g., Nd: Glass (1.05–1.06 μm), Nd: YLF (1047 nm), Yb: Glass, or Yb: YAG (~1030 nm).

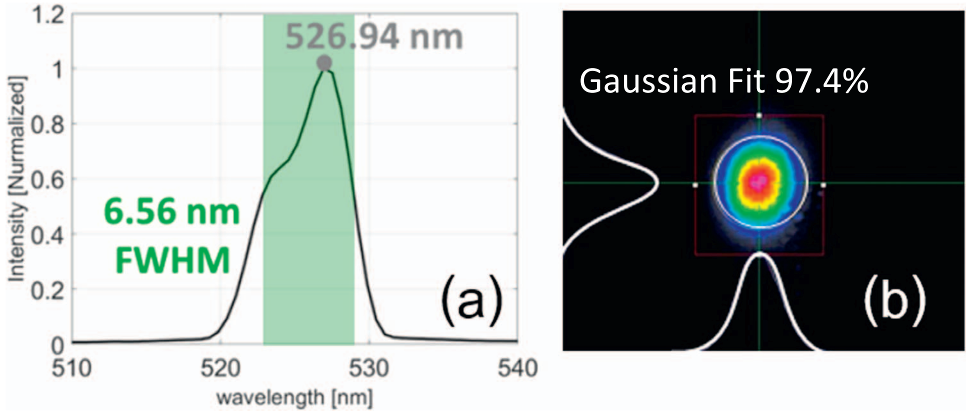

Figure 3. Experimental SHG outcome: (a) SHG spectrum centered at 526.94 nm, and 6.56 nm FWHM. (b) SHG beam shape with 97.4% Gaussian fit.

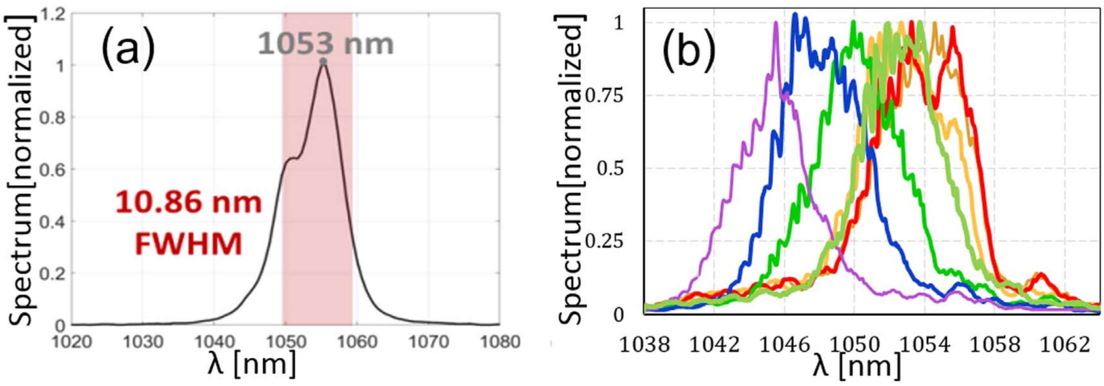

Figure 4. Experimental OPA spectrum: (a) Idler spectrum correlated to 526.5 nm SHG (b): Idler output spectra, obtained for different phase match (PH.M.) cases related to crystal angle tilt.

Table 1. Comparison of typical characteristics of frequency conversion, specifically second harmonic of 1 μm incident light.

	Efficiency	Spatial beam shape	Bandwidth
AFC	~40%	97.4% Gaussian fit. Inherent walk-off free	Fully preserved bandwidth (6.56 nm)
Bulk Barium borate (BBO) crystal	>26.5 [33]	Walk- off angle of ~55 mRad [34]	Bandwidth preservation under some conditions [33]. Needs large phase matching, very short crystal, at the expense of efficiency.
Periodically Poled $LiNbO_3$ (PPLN) [35]	~20%	Potentially Gaussian. Inherent walk-off free	Not fully preserved (4.7 nm out of 11.2 in the first harmonic)

To estimate the contrast change, a comparison between the 1 μm fiber CPA beam that derived the pulse, and the idler output was performed. We specifically estimated the CP that was observed in the few ps regime. The available diagnostics tool was an SHG FROG with a few picoseconds window around the main peak. The dynamic range was limited in this case by the FROG's electronics, nominally specified to ~60 dB. The retrieved estimations and results are shown in figures 5(a) and (b).

The red and green curves in figure 5(a, linear y scale) and (b, power y scale) represent a comparison between the measured idler temporal shape and the CPA beam respectively, showing clear side features suppression and thereby time profile improvement. The CPA pulse structure, shown in figure 5((a), (b), green), results from the seed pulse's specific evolution via the CVBG stretcher and grating compressor, material and fiber dispersions all operating in conjunction. Specifically, figure 5(b) shows a −10 dB pre-pulse in the CPA pulse located ~2.5 ps prior to the main peak, as a result of non-perfectly compensated dispersions whose post suppression process is

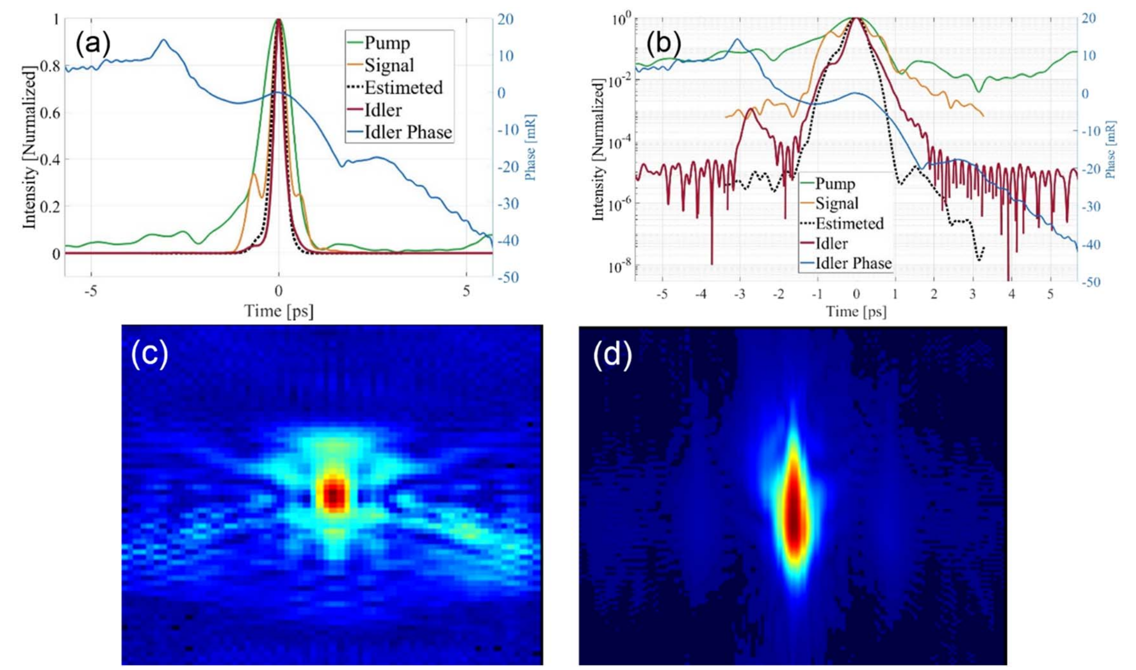

Figure 5. Idler temporal measurements: (a) Linear and (b) Power scale of temporal pulses shapes. Green: CPA after compression (480 fs); Red: idler out of OPA (283 fs); Blue: idler temporal phase; Orange: measured signal after a slight stretching; Black: Estimated Idler: $I_{CPA} \cdot I_{CPA} \cdot I_{signal}$. (c): CPA and (d) idler 2D FROG trace retrievals correspondingly, showing clear side features suppression.

referred below. The dispersion orders of the stretcher and compressor were evaluated numerically to be: 16.4×10^6 versus -16.6×10^6 [fs^2], and -36.07×10^6 versus $+116 \times 10^6$ [fs^3] for the 2nd and 3rd orders, for the CVBG and grating pair respectively. With an estimated few radians of B-integral, the retrieved CPA pulse shape seems to reasonably agree with the result. Based on the FROG retrieval, a 283 fs idler pulse duration was obtained (figure 5(a)), with a potential of 250 fs FTL, supported by the slight spectral phase curve of ~0.2 Radians within the −3 dB time range. Figure 5(a), representing the idler on a linear scale, one can readily note that major parts of the side features were washed out. This well supports the approach in which the idler is the throughput of the double-cleaning process: the pump generation in the AFC being the first cleaning mechanism, and a sequential seed interaction in the secondary crystal, being the additional cleaning stage. To better observe finer details, under the limit of the FROG's spectrometer's dynamic range (10^6), figure 5(b) is presented on a power scale. It can be seen that the side features that were viewed in the CPA pump pulse were suppressed to between 30 to 40 dB when viewed in the idler pulse, measured in the range of up to 6 ps preceding the leading edge, and similar ratios in the trailing edge. In addition, we compared the resulted idler's temporal shape to the expected idler according to equation (2) by multiplying the signal's temporal shape (figure 5(a) orange) with a squared value of the measured CPA pulse (figure 5(a) green), which is the approximation to the SHG pump. The results are presented in figure 5. In the black curve. The difference between the measured and calculated idler can be observed in the power scale in figure 5(b), showing an overall good agreement. As one can readily observe in figure 5(b), The majority of the −10 dB/−2.5 ps pre-pulse mentioned above passed substantial suppression to ~−30 dB in the experiment. The estimated idler, however, is displayed with 20 dB suppression. This smoother manner, only noticeable on a power scale, could be due to some limited spectral filtration ($T_{SHG} = 0.25\%$, $T_{1\mu m} = 98\%$) and polarization extinction ratio at the exit beam splitter (T_P:$T_S > 1000$:1), allowing some unfiltered pump and signal to merge with the output idler.

8. Conclusions

We demonstrated suppression of unwanted side features as well as typical CP trace, at the near vicinity of the main peak, being a nuisance in high-intensity laser-material experiments. We proposed a path for exploring coherent pedestal pulse profile cleaning in an OPCPA by implementing AFC crystals, applied here for pump generation. The pump from the AFC yielded nearly 40% conversion efficiency with a Gaussian spatial beam profile, practically full incident pulse spectral conversion, and good idler efficiencies of >10% to 18% (varying with output wavelengths) with respect to the SHG pump energy (around 800 nJ). We proof-tested the nonlinear AFC structure, designed in-house by the Femto-Nano lab group, in the presented short OPCPA system to support applications that demand temporal pulse shape improvement. Applications like, e.g. generating high harmonics from solids or noble gases, X-Ray production from laser-solid interactions, or laser particle acceleration (either sheath-acceleration or inverse-Compton approaches) can pronouncedly benefit from such enhanced pulse properties. The OPCPA pulses showed smoother profile with up to 40 dB suppression in the unwanted coherent pedestal features. Furthermore, the AFC could assist with tuning the output idler pulse central frequency, which broadens its usability in various 1 μm amplifiers or OPCPAs. Such a clean pulse result suits the demand for high contrast seed into multi-stage CPA and OPCPA lasers. We stress out that further branches of this approach can be developed. Amongst are, e.g., implementing broadband AFC in the OPA stage itself, applying higher energies as well as better dedicated AFC materials and designs, larger dynamic range tests, utilizing further directions, e.g. apodization. With such further future advances and material selection, AFC contributions can evolve to show pronounce advantages, and are believed to further contribute to the field of pulse shaping and contrast improvement.

Acknowledgments

The authors would like to thank and acknowledge the joint Pazy IAEC-UPBC research fund.

Data availability statement

All data that support the findings of this study are included within the article (and any supplementary files).

ORCID iDs

Zaharit Refaeli https://orcid.org/0000-0001-9176-947X
Gilad Marcus https://orcid.org/0000-0003-1905-9187

References

[1] Ghimire S and David A R 2019 High-harmonic generation from solids *Nat. Phys.* **15** 10–6
[2] Sánchez I, Lera R, Ruda J, Gonzalez J B, Ruiz F, Lopez D and Ruiz-de la Cruz A 2018 Experimental study of proton acceleration from thin-foil on a table top Ti:Sapphire *J. Phys. Conf. Ser.* **1079** 012001
[3] Maine P, Strickland D, Bado P, Pessot M and Mourou G 1988 Generation of ultrahigh peak power pulses by chirped pulse amplification *IEEE J. Quantum Electron.* **24** 398–403
[4] Osvay K, Csatári M, Ross I, Persson A and Wahlström C 2005 On the temporal contrast of high intensity femtosecond laser pulse *Laser Part. Beams* **23** 327–32
[5] Danson C, Neely D and Hillier D 2014 Pulse fidelity in ultra-high-power (petawatt class) laser systems *Hi Pow. Laser Sci. and Eng.* **2** e34
[6] Tang Y, Hooker C, Chekhlov O, Hawkes S, Collier J and Rajeev P 2014 'Transmission grating stretcher for contrast enhancement of high power lasers *Opt. Exp.* **22** 29363–74
[7] Kane S and Squier J 1997 Grism-pair stretcher–compressor system for simultaneous second-and third-order dispersion compensation in chirped-pulse amplification *JOSA* B **14** 661–5
[8] Chen R *et al* 2019 Highly-dispersive mirrors with advanced group delay dispersion *IEEE Photonics Technol. Lett.* **32** 113–6
[9] Singh M and Raghuwanshi S K 2015 Effect of higher order dispersion parameters on optical millimeter-wave generation using three parallel external optical modulators *J. Appl. Phys.* **117** 023116
[10] Dorrer C *et al* 2015 OPCPA front end and contrast optimization for the OMEGA EP kilojoule, picosecond laser *J. Opt.* **17** 94007–94007
[11] Itatani J, Faure J, Nantel M, Mourou G and Watanabe S 1998 Suppression of the amplified spontaneous emission in chirped-pulse-amplification lasers by clean high-energy seed-pulse injection *Opt. Commun.* **148** 70–4
[12] Petrov G I, Albert O, Etchepare J and Saltiel S M 2001 Cross-polarized wave generation by effective cubic nonlinear optical interaction *Opt. Lett.* **26** 355–7
[13] Dubietis A, Jonušauskas G and Piskarskas A 1992 Powerful femtosecond pulse generation by chirped and stretched pulse parametric amplification in BBO crystal *Opt. Commun.* **88** 437–40
[14] Marcus G *et al* 2005 Generation of a high-energy ultrawideband chirped source in periodically poled $LiTaO_3$ *JOSA* B **22** 620–2
[15] Deng Y *et al* 2012 Carrier-envelope-phase-stable, 1.2 mJ, 1.5 cycle laser pulses at 2.1 μm *Opt. Lett.* **37** 4973–5
[16] Suchowski H, Porat G and Arie A 2014 Adiabatic processes in frequency conversion *Laser Photonics Rev.* **8** 333–67
[17] Suchowski H *et al* 2011 Adiabatic frequency conversion of ultrafast pulses' *Appl. Phys.* B **105** 697–702
[18] Suchowski H *et al* 2013 Octave-spanning coherent mid-IR generation via adiabatic difference frequency conversion *Opt. Express* **21** 28892–901
[19] Suchowski H *et al* 2009 Robust adiabatic sum frequency conversion *Opt. Express* **17** 12731–40
[20] Heese C *et al* 2010 Ultrabroadband, highly flexible amplifier for ultrashort midinfrared laser pulses based on aperiodically poled Mg: $LiNbO_3$ *Opt. Lett.* **35** 2340–2
[21] Krogen P *et al* 2017 Generation and multi-octave shaping of mid-infrared intense single-cycle pulses *Nat. Photonics* **11** 222–6
[22] Moses J *et al* 2013 Octave-spanning coherent Mid-IR pulses via adiabatic difference frequency generation *Nonlinear Optics* (https://doi.org/10.1364/NLO.2013.NF1A.6)
[23] Heese C *et al* 2012 Role of apodization in optical parametric amplifiers based on aperiodic quasi-phasematching gratings *Opt. Express* **20** 18066–71

[24] Mayer B W *et al* 2013 Sub-four-cycle laser pulses directly from a high-repetition-rate optical parametric chirped-pulse amplifier at 3.4 μm *Opt. Lett.* **38** 4265–8

[25] Phillips C R and Fejer M M 2010 Efficiency and phase of optical parametric amplification in chirped quasi-phase-matched gratings *Opt. Lett.* **35** 3093–5

[26] Heese C *et al* 2011 High-energy picosecond Nd: YVO 4 slab amplifier for OPCPA pumping *Appl. Phys.* B **103** 5–8

[27] Phillips C R, Langrock C, Chang D, Lin Y W, Gallmann L and Fejer M M 2013 Apodization of chirped quasi-phasematching devices *JOSA* B **30** 1551–68

[28] Yaakobi O, Caspani L, Clerici M, Vidal F and Morandotti R 2013 Complete energy conversion by autoresonant three-wave mixing in nonuniform media *Opt. Express* **21** 1623–32

[29] Porat G and Arie A 2013 Efficient, broadband, and robust frequency conversion by fully nonlinear adiabatic three-wave mixing *JOSA* B **30** 1342–51

[30] Treacy E 1969 Optical pulse compression with diffraction gratings *IEEE J. Quantum Electron.* **5** 454–8

[31] Willardson R K *et al* 1998 *Nonlinear Optics in Semiconductors I: Nonlinear Optics in Semiconductor Physics I* (New York: Academic)

[32] Ma J *et al* 2012 Numerical study on pulse contrast enhancement in a short-pulse-pumped optical parametric amplifier *Opt. Commun.* **285** 4531–6

[33] Hong C *et al* 2017 Second harmonic generation based on a 1 μm femtosecond fiber CPA system *Conf. on Lasers and Electro-Optics/Pacific Rim* (Optical Society of America) (https://doi.org/10.1109/CLEOPR.2017.8118957)

[34] Akbari R and Major A 2013 Optical, spectral and phase-matching properties of BIBO, BBO and LBO crystals for optical parametric oscillation in the visible and near-infrared wavelength ranges *Laser Phys.* **23** 035401

[35] Arbore M A *et al* 1997 Frequency doubling of femtosecond erbium-fiber soliton lasers in periodically poled lithium niobate *Opt. Lett.* **22** 13–5